Organized States Arising from Compression of Single Semi-Flexible Polymer Chains in Nanochannels

Lili Zeng and Walter W. Reisner*

Department of Physics, McGill University,

3600 University Street, Montreal, Quebec H3A 2T8, Canada

(Dated: March 30, 2023)

Abstract

We use molecular dynamics (MD) simulation to probe the non-equilibrium physics of single nanochannel-confined semi-flexible polymers in a homogeneous flow field. The flow field compresses the polymer against the end of the nanochannel, simulating an experiment of a nanochannel confined chain compressed against a slit barrier. The flow-based compression gives rise to a packing of the chain against the channel end that possesses a striking organization, consisting of interweaving of folds and circular coils. For stiff chains at low flow, we find that the organization is dominated by repeated hairpin folds. For stiff chains at higher flow, we observe that circular coils arise along with the folds, with folding and coiling domains becoming interwoven at the highest flow speeds. Chain organization is retained even when the chain persistence length is on order of the channel width. We show that the global polymer organization, consisting of a number of defined folds and coiled loops, arises from the minimization of the total chain free energy.

I. INTRODUCTION

Highly organized states can arise in confined systems of single semi-flexible macromolecules. For example, a single semi-flexible polymer chain confined in a spherical cavity at high enough density organizes itself into layers of stacked perpendicular spools [1–3]. This spooling phenomenon is highly significant biologically, arising when $\sim 10 - 100\,\mathrm{kbp}$ of phage dsDNA is packaged inside viral capsids $\sim 100\,\mathrm{nm}$ in diameter. Concentric spools are observed at low densities, while at higher densities additional morphologies emerge, resembling topological links [1].

Nanofluidic systems based on nanochannels have emerged that model experimentally the behavior of DNA at high compression. Nanochannels are well-defined, simple systems where all parameters can be controlled. Studying polymers in nanochannels is a fruitful method to understand complex behaviours seen *in vivo*. In the nanochannel experiments, compression is induced in a non-equilibrium process via either an optically trapped sliding bead piston or hydrodynamic flow against a barrier which blocks the polymer but lets the fluid flow through via a very thin slit. Recent studies using nanochannels have shown that a simple partial differential equation model can capture the time-dependent concentration profile along the

---

* reisner@physics.mcgill.ca

channel axis [4, 5]. In addition, knots are generated at high compression; the knot-factory technique is now used to produce knots for further study of knot dynamics, diffusion, and interactions in confinement [6–8].

One intriguing question is whether, at sufficiently high compression, the organized states found in phages can be artificially produced in the nanochannel system. Previous simulation work has shown that non-equilibrium compression in the presence of confinement can give rise to organized states of single semi-flexible macromolecules. In the limit of very high chain rigidity, where the persistence length P is comparable to the contour length L, a symmetrically compressed chain transitions from a regime of disordered Odijk deflections to a structured helical state. Upon further compression, the chain folds over itself and transitions from a disordered deflection state containing two parallel polymer strands to a double helical state [9]. At lower chain rigidity, but with P still greater than the channel diameter D, a chain compressed from one end via a sliding piston forms repeated hairpin folds. The number of folds increases with the sliding velocity v [10]. Scaling relations have also been studied for semi-flexible polymers in nanochannel confinement under compression [11].

A full picture has yet to emerge, however, regarding the full spectrum of possible organized states of a compressed semi-flexible chain, as well an understanding of how these states arise in a non-equilibrium compression process. So far, while chain organization has been observed via simulation for the regime where $P > D$, evidence is lacking that organization might arise as well in the regime $P \leq D$, which is easier to reach in experiments. Here we use molecular dynamics (MD) simulations to probe the non-equilibrium physics of single nanochannel confined semi-flexible polymers compressed against a barrier in a homogeneous flow field. We approximate the barrier as perfectly porous to the fluid-flow so that flow can be assumed uniform up to the barrier, an idealization of the experimental slit geometry. Note that, in this case, a chain pushed against the (stationary) barrier by a homogeneous steady flow field is equivalent to a chain pushed at constant speed by a moving (piston) barrier in an immobile fluid (such as performed in Bernier *et al.*). The latter case (moving piston barrier, immobile fluid) can be converted to the former case (stationary barrier, uniform flow) by changing the frame of reference from a frame where the fluid is at rest (and piston moving) to one co-moving with the piston. For high enough P, we observe two distinct types of structures: folds, as observed by Bernier *et al.* [10], and coils, a new phenomenon distinct from helices observed by Hayase *et al.* [9] and also distinct from the spools observed by Curk *et al.* [1] (Figure 1). A fold refers to when a strand of polymer folds over itself into a hairpin, exactly as described by [10] (see Figure 1d-f). A coil is formed when a strand of polymer forms a loop guided by the circular side walls of the cylindrical nanochannel. The plane of the loop is typically perpendicular to the channel axis. When multiple loops are adjacent along the channel axis, they stack compactly side-by-side, rather than forming a true helix as in Hayase *et al.* [9], or a thick spool with loops inside loops within the same spool layer, as in Curk *et al.* [1] and Petrov *et al.* [3] (see Figure 1g-i). We find that folds dominate in the low v regime, while coils dominate in the high v regime. Interestingly, coils often coexist alongside folds; the coils wrap around the folds, similar to a two-layer spool observed by Curk *et al.* [1]. Notably, we also find that coils and folds arise even for $P < D$.

Transient analysis reveals that for a sufficiently stiff chain at high enough flow, folds and coils form as soon as the chain end touches the barrier, but for stiff chains at high flow the initial mixture of folds and coils can be slanted relative to the channel axis. A distinct time-scale then exists for the chain configuration to decay into an organized series of coils and folds.

We believe that the global polymer organization, consisting of a number of defined folds and coiled loops, arises from the minimization of the total chain free energy, which consists of a bending energy component and a flow potential component. Our theoretical model, based on a simplified chain configuration with idealized folds and coils, predicts the simulation results with good agreement for sufficiently high chain rigidity.

A note about terminology: we use the term ‘loop’ to refer to single circular loops perpendicular to the channel axis; we use ‘coil’ to refer to the whole aggregate of loops.

II. MODEL AND SIMULATION DETAILS

Our simulations are performed using the MD package *ESPResSo* [12]. Our implementation consists of a bead-spring model of a polymer with the monomers interacting via excluded volume (EV), a finite extension nonlinear elastic (FENE) spring potential, and a bond-bending potential enabling variation of P. We tested our MD system for chains in bulk and confined in open channels, and reproduced the scalings for the Flory radius in bulk, and the chain extension in cylindrical channels in the de Gennes/extended de Gennes regime

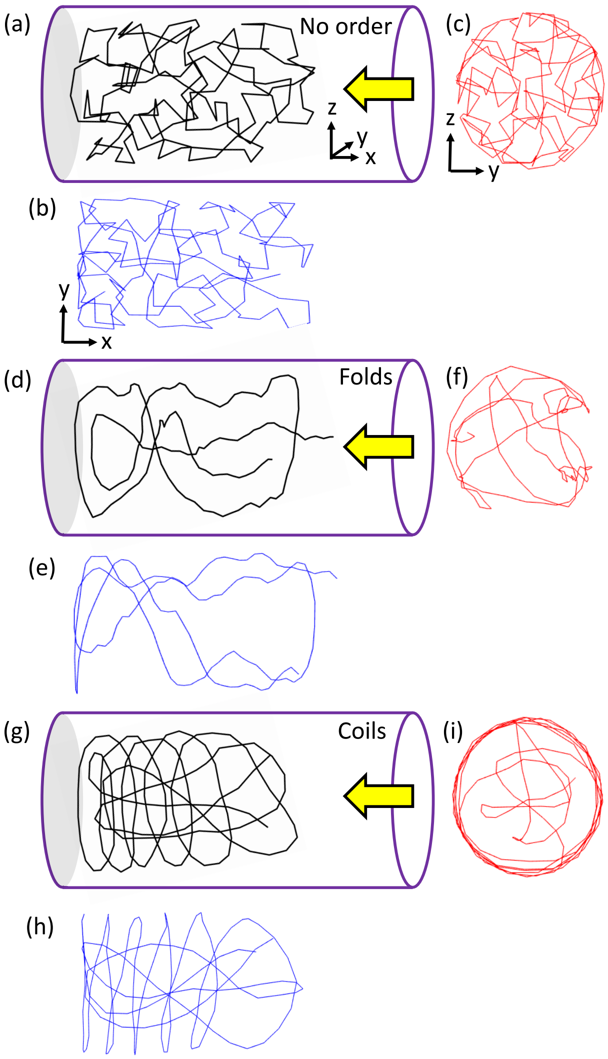

FIG. 1. (a-c) Snapshot of a $P = 0$ configuration. (d-f) Snapshot of a high P, low v configuration. (g-i) Snapshot of a high P, high v configuration. (a,d,g) show the 3D representation of the chain, with (b,e,h) being a longitudinal projection and (c,f,i) a transverse projection.

($P < D$) and in the Odijk regime ($P > D$). We also computed the steady-state density profile for flow-compressed chains in closed channels and found them comparable with experiment, showing the applicability of the MD simulation method to study non-equilibrium dynamics of confined polymers.

We keep the channel width D, the monomer size σ, and the number of monomers N fixed, but allow P and v to vary, so as to explore chains of different stiffness subject to different flow velocities. The EV interaction between any two monomers separated by a distance of r is given by a short-range truncated Lennard-Jones (LJ) potential, also called the Weeks–Chandler–Andersen (WCA) potential [13]:

$$\begin{aligned} U_{WCA}(r) &= 4\epsilon\left[\left(\frac{\sigma}{r}\right)^{12}-\left(\frac{\sigma}{r}\right)^{12}+\frac{1}{4}\right] && \text{if } r < 2^{1/6}\sigma \\ &= 0 && \text{otherwise} \end{aligned} \tag{1}$$

where ϵ is the interaction strength. The successive monomers are connected by a finite extension nonlinear elastic (FENE) spring potential [14]:

$$U_{FENE}(r) = -\frac{1}{2}kR_0^2\ln\left(1-\frac{r^2}{R_0^2}\right) \tag{2}$$

where k is the interaction strength and R_0 is the maximum allowed bond length. The parameters k, R_0, ϵ, and σ determine the bond length. The chain stiffness is controlled by a three body bond-bending potential:

$$U_{bend} = \kappa[1-\cos(\theta-\theta_0)] \tag{3}$$

where θ, shown in Figure 2a, is the angle between two successive bonds, κ is the interaction strength, and θ_0 is the equilibrium bond angle. In three dimensions, for $\kappa \neq 0$, the persistence length P of the chain is related to κ via [15]

$$P = \frac{\kappa\sigma}{k_BT} \tag{4}$$

where k_BT is the thermal energy. The confining walls of the cylindrical nanochannel, including its ends, interact with the monomers also via the WCA potential, but with interaction strength $\epsilon_{walls} = 20\epsilon$ and interaction length $\sigma_{walls} = 0.2\sigma$. As for the applied flow field, it is defined by a force on each monomer

$$\vec{F} = -\gamma_v(\vec{v}-\vec{u}) \tag{5}$$

where $\gamma_v = \gamma$ is a friction factor, $\vec{v}$ is the flow velocity, and $\vec{u}$ is the monomer velocity. There are no hydrodynamics involved in the simulations as they are expensive to compute, and their effect can be taken into account by normalizing the friction factor [10].

The MD simulation propagates forward using the Langevin dynamics equation of motion. For monomer i,

$$m\ddot{r}_i = -\nabla(U_{WCA}+U_{FENE}+U_{bend}+U_{WCAwall})+\vec{F}-\gamma\dot{r}_i+\sqrt{6\gamma k_BT}\eta_i(t) \tag{6}$$

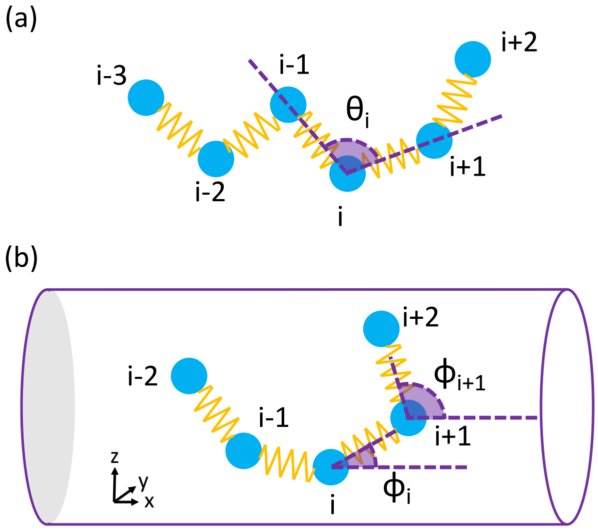

FIG. 2. (a) Diagram showing a bead-spring model chain with the angle between bonds θ, from which the bending energy is calculated. (b) Diagram showing a bead-spring model chain with the angle between each bond and the channel axis ϕ, which we use in our analysis.

where m is the monomer mass, r_i is the monomer position, γ is the friction coefficient, k_BT is the thermal energy, and $\eta_i(t)$ is a Gaussian random force with zero mean and variance of one.

For all our simulations, we set $\sigma = 1$, $N = 150$, $D = 6$, $m = 1$, $\gamma = 1$, and $k_BT = 0.2$. For the WCA potential, we set $\epsilon = 1$; for the FENE potential, we set $k = 10$ and $R_0 = 2$; and for the bending potential, we set $\theta_0 = \pi$. We vary κ between 0.24 and 3.2, corresponding to persistence lengths of 1.2 and 16. We also perform simulation with no bending energy, or $P = 0$. Finally, we vary v ($\vec{v} = (v, 0, 0)$) by two orders of magnitude, between 0.002 and 0.2.

For a given simulation run, we initialize our polymer in a straight line in the center, along the axis of the cylindrical channel. We set a fixed amount of time for the system to reach equilibrium ($t = 1 \times 10^6$, corresponding to 5×10^8 iterations of $\Delta t = 0.002$ each). We ensure that equilibrium is reached by observing when the chain extension stabilizes (which usually happens within half of the fixed preset time). We then apply the homogeneous flow field to compress the chain (for another $t = 1 \times 10^6$). We save the polymer configuration (x, y, and z positions for each monomer) every time interval $\Delta t = 50$. We run such simulations over a range of 6 bending energies and 12 flow velocities, with 3 independent simulations run for each set of parameters v and κ, for a total of 216 runs of about 15-20 hours each. These simulations were run on Compute Canada's supercomputer cluster *Beluga*.

III. SIMULATION RESULTS

In order to better visualize the chain conformation, we introduce two representations in addition to simple 2D or 3D position plots. These include *longitudinal position* plots, or monomer position along the channel axis x vs monomer number s, and *angular* plots, or bond angle with respect to the channel axis vs bond number s'. Examples of longitudinal position plots are shown in Figure 3d,i,n for a completely disordered regime, a folded regime, and a regime containing co-existing coils and folds. Figure 3d shows an example longitudinal position plot for a chain with zero bending energy, giving rise to the disordered behavior expected for a confined self-avoiding chain. Figure 3i shows an example longitudinal position plot for a chain with high bending energy and low flow velocity; zigzag like structures are observed in the plot, indicative of hairpin folds and comparable to those observed by Bernier *et al.* [10]. The line segments on either side of the zigzag's v-shaped edge represent chain portions undergoing Odijk deflections with no-backfolding, i.e. that basically propagate in a directed fashion down the channel axis. Finally, Figure 3n shows an example longitudinal position plot for a chain with high bending energy and high flow velocity. This plot contain staircase like structures along with the zigzags folds. Examining the 3D configuration plot for this chain (Figure 3k) suggests that these staircase like structures are indicative of repeated loops around the cylindrical confining surfaces.

To add further insight into the chain configuration, we introduce angular plots, depicted in Figure 3e,j,o (a schematic defining the angle ϕ is shown in Figure 2b). The angular plots are generated by calculating the bond vector between consecutive monomers, and then finding the angle the bond vector makes with the channel axis (there are 150 monomers, and therefore 149 bonds, each at position $s'_i = (s_i + s_{i+1})/2$). The angles range between 0 and π, with a value of $\pi/2$ indicating a bond perpendicular to the channel axis. For the disordered chain configuration in Figure 3e, the values of ϕ are distributed randomly as expected. In Figure 3j, the ϕ values alternate between values close to 0 and values close to π; this arises because the straight edges flanking the v-shaped edge in the corresponding longitudinal position plot (Figure 3i) represent polymer segments directed in opposite directions along the channel axis (corresponding to $\phi = 0$ and $\phi = \pi$). Finally, in Figure 3o, the coiled part of

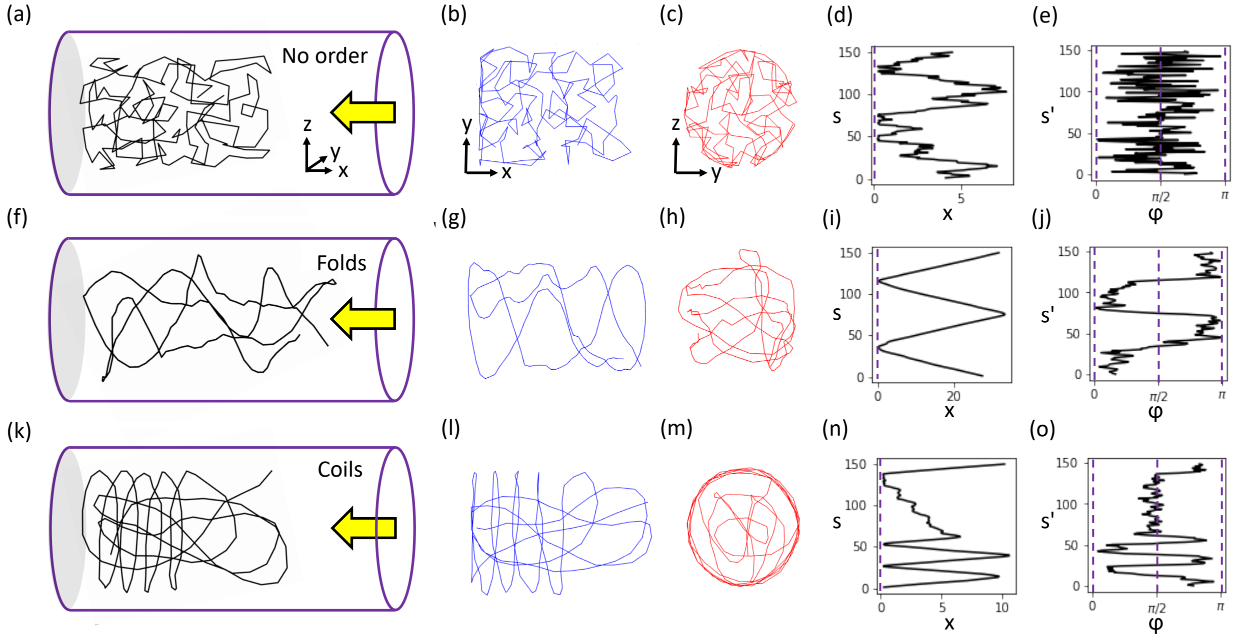

FIG. 3. (a-e) Snapshot of a $P = 0$ configuration. (f-j) Snapshot of a high P, low v configuration. (k-o) Snapshot of a high P, high v configuration. (a,f,k) show the 3D representation of the chain, with (b,g,l) being a longitudinal projection and (c,h,m) a transverse projection. (d,i,n) show the monomer number s vs the channel axis position x (barrier position at dashed line), while (e,j,o) show the bond number s' vs bond angle ϕ.

the chain (staircase section in Figure 3i) have values close to $\pi/2$ as loops are perpendicular to the channel axis.

These longitudinal position and angular plots give information on the configuration of the chain in two ways. As they are more compact, they can be plotted for consecutive snapshots to understand the history of the chain configurations (which will be investigated further in subsection A, Chain History). Moreover, as coils and folds take different angular values in the angular plots, these values can be extracted to calculate an order parameter, which indicates the level and type of ordering of each steady-state configuration (this will be investigated further in subsection B, Order Parameter).

A. Chain History

Chain histories are represented by plotting longitudinal positions snapshots taken at incrementally increasing times. Each line in Figure 4 and 5 represents a snapshot, and consecutive snapshots over time are shifted by a small horizontal distance for better visualization.

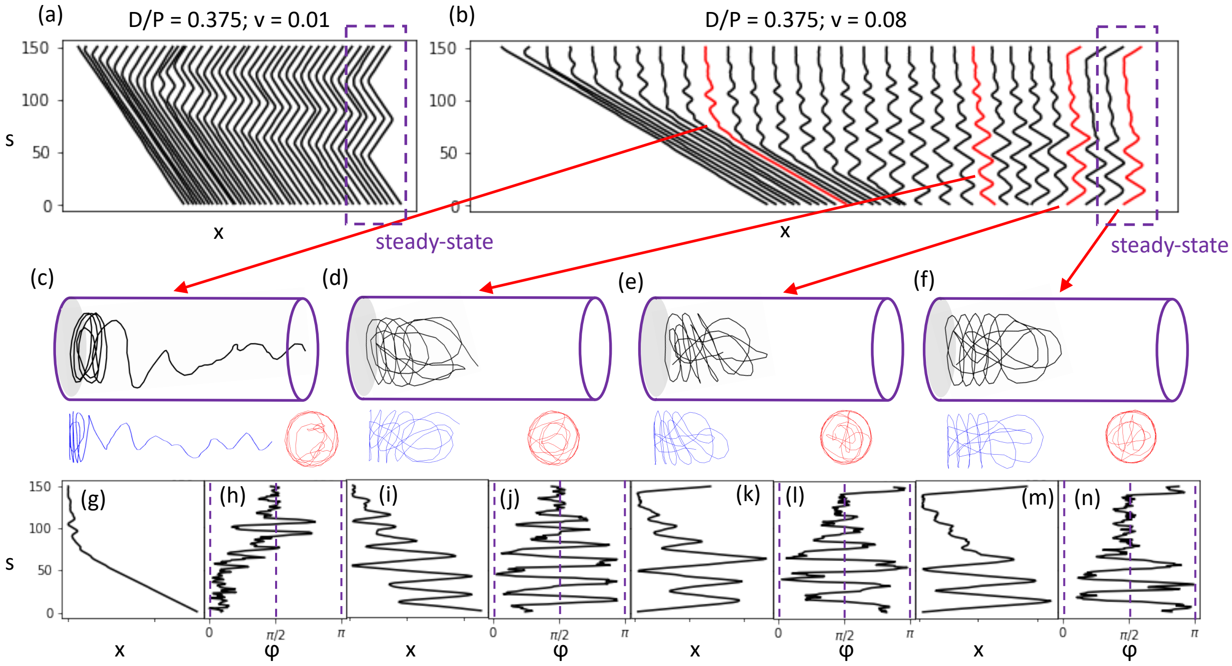

FIG. 4. Diagrams showing the transient chain history, with the formation of folds in (a), and formation of coils and folds in (b). Each line in a subplot shows a single snapshot of the monomer number s vs monomer channel axis position x. Lines from left to right represent snapshots at increasing time. An increasing x shift is added to the lines for increasing time for better visualization. (c-f) Snapshots of chain configuration at different times in transient chain history, with (g,i,k,m) showing expanded longitudinal position plots and (h,j,l,n) showing angular plots for each snapshot.

Transient chain histories show us that configurations with folds form exactly the same way as described by Bernier *et al* [10], with repeated folds arising as V-shaped kinks in the longitudinal position plot (see Figure 4a). For higher flow values, coils can form in addition to folds. Figure 4(b-n) shows an example compression event where folds and coils both form, including longitudinal positions plots over the compression history (Figure 4b), configuration snapshots (Figure 4c-f) and angular plots (Figure 4h,j,l,n). Note that the coils form early in the compression process and arise close to the barrier, corresponding to the portion of the chain feeling the greatest compressive force. Also, note that the coils are initially slanted (Figure 4d-e), yet eventually in a sudden fashion get pulled flat (Figure 4f), suggesting that the slanted coil configuration represents an intermediate in the compression process (and the perpendicular configuration is the final state). Note that the slanted coil intermediate lasts $< 10\%$ of the total simulation run. For the rest of the manuscript we choose to focus on the long-time steady-state behaviour (shown as dashed boxes in Figure 4a-b), leaving the details of the transient behavior involving combined folds and coils for a future study.

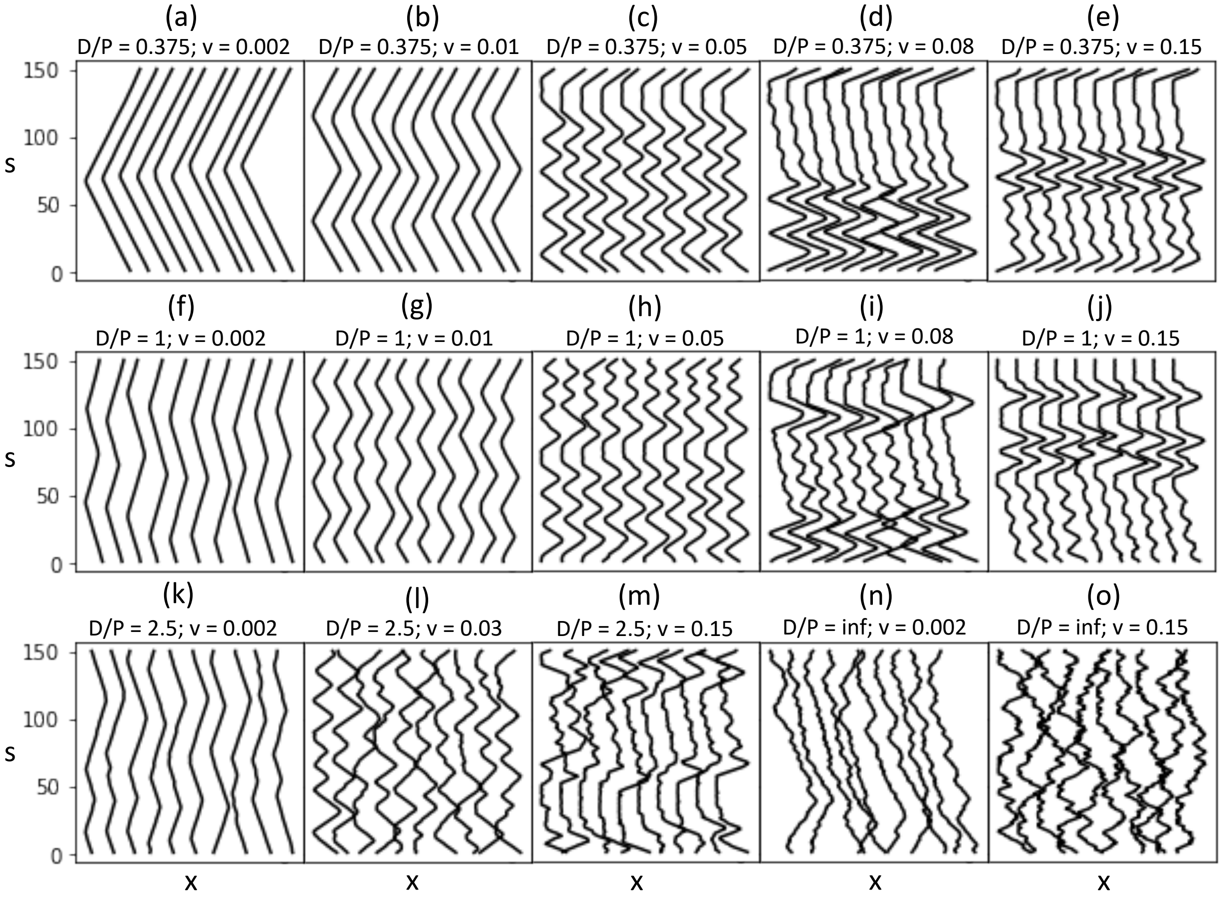

FIG. 5. (a-e) Histories for $P > D$ from low v to high v. (f-j) Histories for $P = D$ from low v to high v. (k-m) Histories for $P < D$ from low v to high v. (n-o) Histories for $P = 0$ for low v and high v. Each line in a subplot shows a single snapshot of the monomer number s vs monomer channel axis position x. Lines from left to right represent snapshots at increasing time. An increasing x shift is added to the lines for increasing time for better visualization.

Figure 5 shows the long-time steady-state behaviours for different P and v values. For the highest P and lowest v value (Figure 5a), only a single fold forms and the fold position shows only a small degree of fluctuation along the chain contour. For a slightly higher v (Figure 5b), three folds form, with the same degree of fluctuation in fold position. For intermediate v values (Figure 5c,d), one or more loops form originating from the chain end that is closest to the barrier and feels the greatest compressive force. Finally, for high v values (Figure 5e), loops form interspersed with folds. For different equivalent runs in this parameter regime, the total numbers of loops and folds remain constant, but their relative position along the chain contour vary.

For $D = P$ (Figure 5f-j), the same trend holds, but we can see that the position of the folds and coils along the chain contour fluctuates to a greater degree. For $D > P$ (Figure 5k-m), folds and coils continually form, dissolve, and move along the chain contour. However, the total numbers of loops and folds remain more or less constant over time. Finally, for $P = 0$ (Figure 5n-o), as expected the configurations become completely disordered.

These observations suggest that the chain adopts a fixed number of folds and loops for a given set of parameters ($P \neq 0$).

B. Order Parameter

We can use our angle plots to introduce an order-like variable η to quantify the type and degree of organization experienced by the compressed chain (i.e. folded or coiled). We define the order parameter by summing the angle ϕ relative to $\pi/2$ for all bonds:

$$\eta = \sum_{i=1}^{N-1} |\phi_i - \pi/2|. \tag{7}$$

We expect η to be close to 0 for coiled configuration and close to $\pi/2$ when folds dominate. For a random configuration or for a combination of folds and coils, η should be somewhere in between 0 and $\pi/2$.

We plotted η for variable v and D/P values in Figure 6a. We observe that for $P = 0$, η is roughly constant as a function of v and has a value of approximately 0.6. As P increases, the slopes of each η vs v plot become steeper and more negative. In particular, we observe that lower v values have corresponding η values that are higher than 0.6, while higher v values have η's below 0.6. Evidently, as we expect low P values correspond to more disordered states (constant $\eta \approx 0.6$) while higher P values have folded configurations at low v (high η)

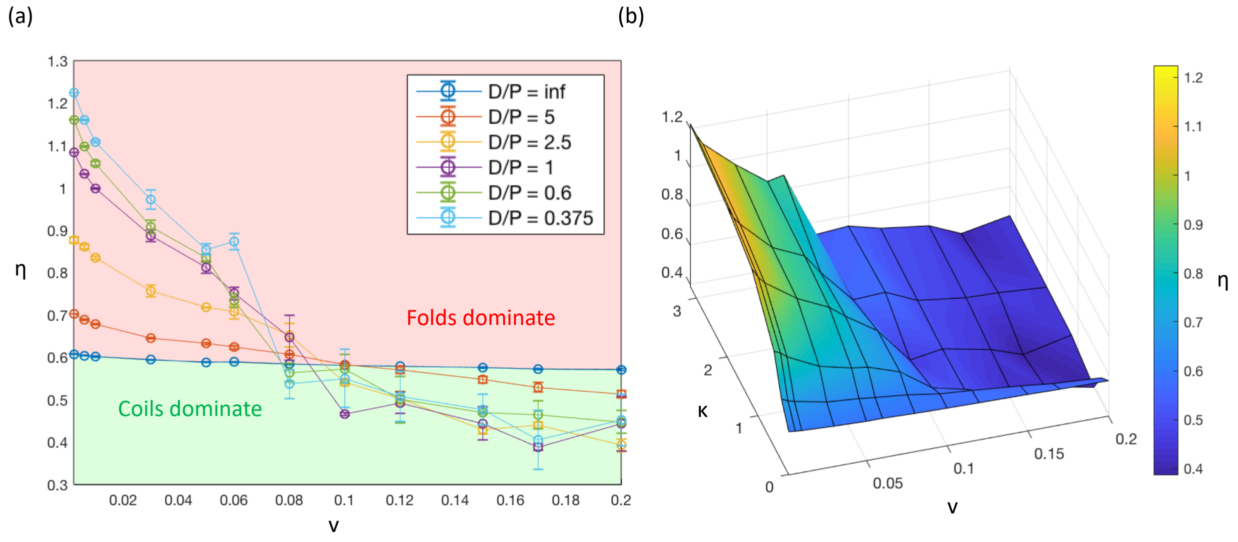

FIG. 6. (a) Order parameter η as defined by Equation 7 plotted for different v and D/P values. Error bars give error on the mean for three independent runs. (b) Order parameter η vs bending energy κ and vs v visualized as a 3D plot.

and coiled configurations at high v (low η). The critical η-value $\eta = 0.6$ acts as a natural boundary between pure folded and coiled regimes. In addition, notice that organization starts appearing even for $D/P > 1$ (corresponding to $\kappa < 1.2$ in Figure 6b). While chain organization can be readily quantified as consisting of a certain number of folds and loops for $D/P \leq 1$, which will be explored in the next section, such methods break down for $D/P > 1$ where the number of folds and coils are not well-defined due to high chain fluctuations. In this case, the order parameter still reveals a small degree of residual organization.

IV. FREE ENERGY MODEL TO QUANTIFY CHAIN ORGANIZATION

Global chain organization can be inferred from the longitudinal position plot. Folds show up as sharp bends in the plot while loops show up as staircase-like segments (Figure 7a-b). We have been able to directly extract the number of folds and loops for all simulation runs for which $D/P \leq 1$. The clear trend is that both the number of folds and loops increase for increasing v and decreasing P. Note that that the number of loops grows abruptly at a critical v.

We then develop a model for determining theoretically the number of folds and loops

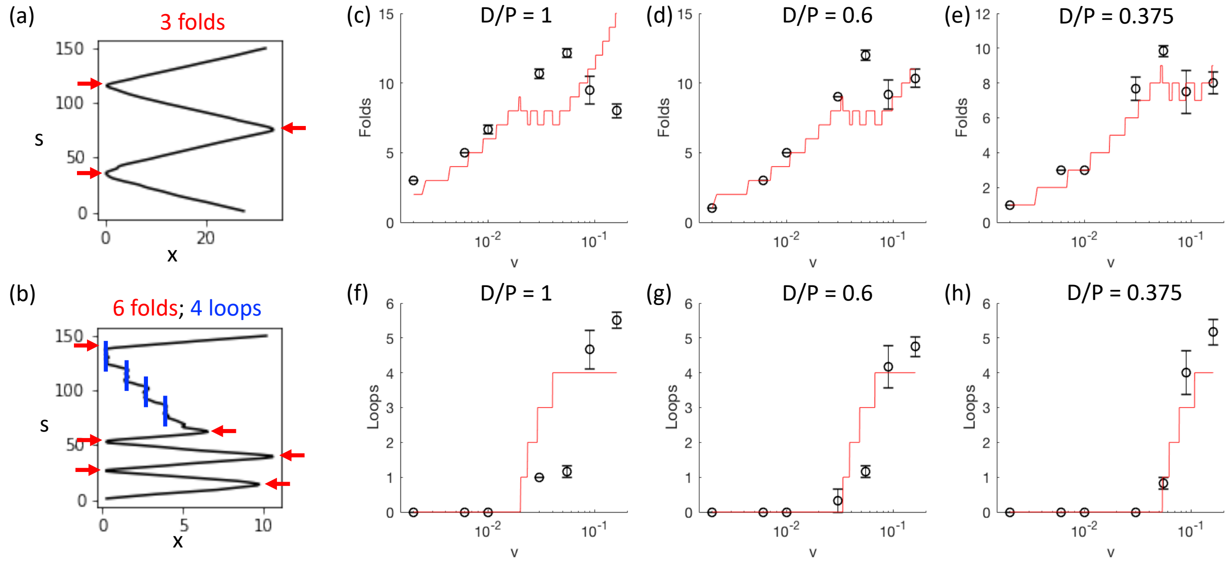

FIG. 7. (a-b) Example configurations where folds are marked in red and loops are marked in blue. In (a), there are 3 folds and 0 loops; in (b), there are 6 folds and 4 loops. (c-e) Number of folds vs. v, for increasing P; (f-h) number of loops vs. v, for increasing P. In (c-h), simulation results averaged over $3-12$ runs shown in black, with error bars representing the standard error on the mean, and fitted theoretical model shown in red.

for a given set of parameters v and P. The model relies on calculating the free energy of idealized chains with different numbers of folds and loops. The theoretical number of folds and loops associated with a set of v and P are the ones that minimizes the free energy.

We assume the chain free energy has two components: the bending energy component and the flow potential component. In the $P \geq D$ regime, the entropy makes a minimal contribution to the total free energy, and we believe it can be safely ignored. The total chain bending energy is the sum over all bonds of the bending energy per bond (Equation 3). In the steady-state configuration, a chain segment will be immobile (on average). The force exerted by the flow on the segment will then be given by Equation 5 with $\vec{u} = 0$, so that the segment will experience a constant flow force $\vec{F}_{flow} = -\gamma_v \vec{v}$. This situation is analogous to a particle in a constant gravitational potential. The potential energy per monomer will be simply $U_{flow} = \vec{F}_{flow} \cdot \vec{x}$ where $\vec{x}$ is the longitudinal vector between the monomer and the closed end of the cylindrical channel. The total flow potential is therefore the potential energy per monomer summed over all monomers.

We calculate the chain free energy using an idealized chain configuration. We first note that a loop consists of ~ 16 monomers, given our channel dimensions ($D = 6$) and monomer size ($\sigma = 1$). We assume each of these 16 monomers have about the same bond angle on average, which we call ϕ_{avg}. Therefore, the contribution due to bending energy of a loop is $16\kappa[1 - \cos(\phi_{avg} - \phi_0)]$. Since each loop is in a plane perpendicular to the flow (our simulations show that the coiled region is not a 3D helix, and each loop is really in a 2D plane, as seen in Figure 3l), each monomer of the loop has the same potential energy. Therefore, the contribution to the flow potential of a loop is $16\gamma_v v x_{loop}$ where x_{loop} is the longitudinal position of the loop with reference to the end of the channel. $x_{loop} = 0, 1\sigma, 2\sigma, 3\sigma...$ for the first, second, third loop, and so on, as each loop is assumed to be stacked on top of the previous one.

Once the free energy contribution of the loops have been calculated, we calculate the free energy of the rest of the chain, which is in folded configuration. We calculate the number of monomers in folded configuration $N_{fold} = N - N_{coil}$ where N is the number of monomers of the whole chain, and N_{coil} is the number of the monomers in coil configuration. We then approximate a configuration of n_f folds as having n_f sections of half-loops (8 monomers at the same angle ϕ_{avg}) and $n_f + 1$ straight sections in the longitudinal direction. The bending energy contribution per fold is therefore $8\kappa[1 - \cos(\phi_{avg} - \phi_0)]$ while the potential energy of each segment of length $L_{seg} = N_{fold}\sigma/(n_f + 1)$ is $\gamma_v v(L_{seg}\sigma + 1)L_{seg}\sigma/2$, using the formula for the sum of consecutive integers.

Using these approximate formulas, we can calculate the total free energy for different numbers of loops and folds if parameters v, P, and ϕ_{avg} are known. The theoretical numbers of loops and folds for a set of parameters are the numbers that minimize the total free energy. Notice that these numbers of loops and folds are discrete in our model. In practice, we set ϕ_{avg} as a fitting parameter as we fit the 2D curves for loop and fold numbers to the simulation results. We also tried using two other fitting parameters: γ_v and ϵ_{pen}, which adds an increasing penalty to the bending energy of a fold for increasing numbers of folds. The rationale of the penalty term is that the larger the number of folds, the tighter the space that each fold occupies, hence the angle of each bond inside the fold becomes sharper and the bending energy per fold increases. However, fitting the model to simulation data revealed that the two additional fitting parameters were not necessary to capture the chain behaviour.

We find that our free energy model captures the observed trends in fold and loop number from simulations (Figure 7c-h). The detailed shape of the curves for simulation and theory do differ at lower P and higher v, for which there are the highest numbers of folds and loops, and the larger the numbers of folds and loops, the larger the error in our free energy estimate, which is calculated using approximations. However, for high P and low v, the model follows the simulation values quite well. In particular, note that the model captures the abrupt onset of coil formation at a critical flow velocity. Note that the theoretical free energy calculation takes only integer numbers of folds and loops, hence the discrete output of the theoretical model in Figure 7c-h.

As for the fitting parameters, we recover $\phi_{avg} = 139 \pm 2^\circ$ or 2.42 ± 0.04 rad. In comparison, a regular nonagon has interior angles of 140°, while a regular 16-sided polygon has interior angles of 157.5°. We believe the discrepancy is small, and due to the fact that the actual average configurations of the chains in the simulations are tighter than the largest allowed loop in the channel, a fact that was also reported by Odijk and ascribed to entropic depletion effect [16].

V. DISCUSSION AND CONCLUSION

In summary, we have established that under non-equilibrium compression in a cylindrical nanochannel, a semi-flexible chain will self-organize into a complex interweaving of folds and coils. In particular, we have shown that such organization arises even in the case of mildly stiff chains ($P < D$), in contrast to previous findings [10]. Our simulation results take place at an intermediate position in parameter space compared to previous studies. Studies of stiffer chains at lower compression obtained hairpin folds configurations [10], which we have also found. As we increase the compressive flow however, we observe coiling, a new result. These coiled configurations, where loops form along the side walls of the cylindrical channel wrapping around folds in the center of the channel, start resembling the layers of spools observed in high density spherical cavities [1, 3]. Preliminary data indicates that increasing compression further in our simulations could reproduce the multi-domain spools observed by Curk *et al.* and Petrov *et al.*

One interesting question is why Bernier *et al.* did not observe coiled organization. Note that Bernier *et al.* performed their simulations using nanochannels with square cross section for similar values of stiffness and flow. We find that compression in a square nanochannel does not produce a configuration consisting of multiple stacked coils as does compression in circular cross-section channels (Figure 8a-e). Interestingly, simulations in half-cylindrical nanochannels (cross-section is a half-disk) yield half-loops on the curved side of the channel instead of full loops as in cylindrical nanochannels (Figure 8f-j). These results suggest that configurations are geometry-dependent. While having the chain conform roughly to the outer boundary of the channel minimizes the total free energy in every geometry, local regions of high curvature (i.e. sharp corners), give rise to an energy barrier for coil formation. This energy barrier prevents the formation of complete coils for channel cross-sections that possess distinct corners (such as square and half-cylinder channels). Note that cylindrical nanochannels can be made experimentally from silica or other materials, either using a laser-assisted mechanical pulling process [17], or by using a polymeric fiber as a template around which a deposited coating forms a tube [18].

We believe that folds and coils configurations emerge in stiffer chains because they lower the total free energy. We have shown using a simplified model that this explanation is plausible. However, a more detailed free energy model, including the fluctuation of configurations around the energy minimum, more realistic modeling of folds and coils, and the entropic wall-depletion effects, could yield further insights. Moreover, including the energy barrier to coil formation in the model would be necessary to understand configurations in square and semi-circular cross-section channels. There is rich physics in transient behaviours as well, e.g. how coils form and evolve over time; this could be explored in a future study. Finally, future work could more comprehensively map out the compression phase space of where folds, coils, and other possible configurations appear.

ACKNOWLEDGMENTS

This work is supported by the Fonds de recherche du Québec - Nature et technologies (FRQNT) Doctoral Research Scholarship (Award No. 273210), and by the Natural Sciences and Engineering Research Council of Canada (NSERC) Discovery Grants Program (Grant

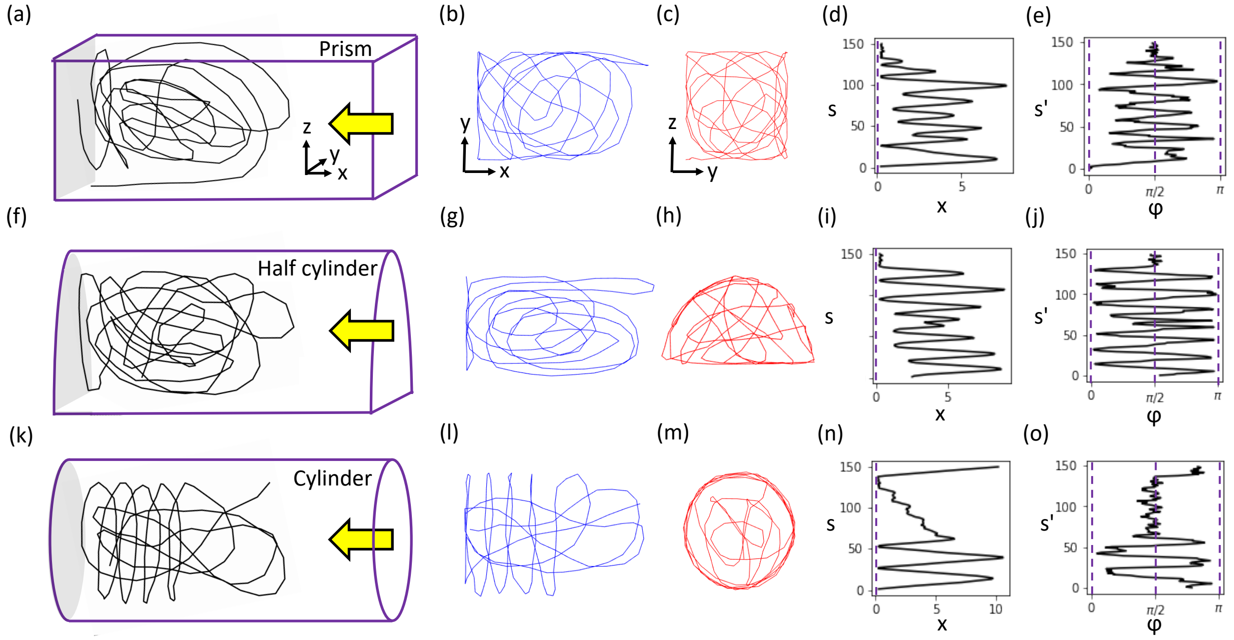

FIG. 8. (a-e) Snapshot of a square prism nanochannel configuration. (f-j) Snapshot of a half-cylinder nanochannel configuration. (k-o) Snapshot of a cylinder nanochannel configuration (identical to Figure 3k-o, reproduced for comparison purposes). (a,f,k) show the 3D representation of the chain, with (b,g,l) indicating a longitudinal projection and (c,h,m) a transverse projection. (d,i,n) show the monomer number s vs the channel axis position x (barrier position at dashed line), while (e,j,o) show the bond number s' vs bond angle ϕ.

No. RGPIN-2018-06125).

[1] T. Curk, J. D. Farrell, J. Dobnikar, and R. Podgornik, Spontaneous domain formation in spherically confined elastic filaments, *Physical Review Letters* **123**, 047801 (2019).

[2] D. Marenduzzo, C. Micheletti, and E. Orlandini, Biopolymer organization upon confinement, *Journal of Physics Condensed Matter* **22**, 283102 (2010).

[3] A. S. Petrov and S. C. Harvey, Packaging double-helical DNA into viral capsids: Structures, forces, and energetics, *Biophysical Journal* **95**, 497 (2008).

[4] A. Khorshid, P. Zimny, D. Tétreault-La Roche, G. Massarelli, T. Sakaue, and W. Reisner, Dynamic compression of single nanochannel confined DNA via a nanodozer assay, *Physical Review Letters* **113**, 268104 (2014).

[5] A. Khorshid, S. Amin, Y. Zhang, T. Sakaue, and W. Reisner, Non-equilibrium dynamics of nanochannel confined DNA, *Macromolecules* **49**, 1933 (2016).

[6] S. Amin, A. Khorshid, L. Zeng, P. Zimny, and W. W. Reisner, A nanofluidic knot factory based on compression of single DNA in nanochannels, *Nature Communications* **9**, 1506 (2018).

[7] Z. Ma and K. D. Dorfman, Diffusion of knotted DNA molecules in nanochannels in the extended de Gennes regime, *Macromolecules* **54**, 4211 (2021).

[8] Z. Ma and K. D. Dorfman, Diffusion of knots along DNA confined in nanochannels, *Macromolecules* **53**, 6461 (2020).

[9] Y. Hayase, T. Sakaue, and H. Nakanishi, Compressive response and helix formation of a semiflexible polymer confined in a nanochannel, *Physical Review E* **95**, 052502 (2017).

[10] S. Bernier, A. Huang, W. W. Reisner, and A. Bhattacharya, Evolution of nested folding states in compression of a strongly confined semiflexible chain, *Macromolecules* **51**, 4012 (2018).

[11] T. Sakaue, Compressing a confined DNA: From nano-channel to nano-cavity, *Journal of Physics Condensed Matter* **30**, 244004 (2018).

[12] F. Weik, R. Weeber, K. Szuttor, K. Breitsprecher, J. de Graaf, M. Kuron, J. Landsgesell,H. Menke, D. Seana, and C. Holm, Espresso 4.0 - an extensible software package for simulating soft matter systems, *The European Physical Journal Special Topics* **227**, 1789 (2019).

[13] J. D. Weeks, D. Chandler, and H. C. Andersen, Role of repulsive forces in determining the equilibrium structure of simple liquids, *The Journal of Chemical Physics* **54**, 5237 (1971).

[14] T. Soddemann, B. Dünweg, and K. Kremer, A generic computer model for amphiphilic systems, *European Physical Journal E* **6**, 409 (2001).

[15] L. D. Landau and E. M. Lifshitz, *Statistical Physics* (Pergamon Press, 1969).

[16] T. Odijk, DNA confined in nanochannels: Hairpin tightening by entropic depletion, *Journal of Chemical Physics* **125**, 204904 (2006).

[17] B. Zhang, M. Wood, and H. Lee, A silica nanochannel and its applications in sensing and molecular transport, *Analytical Chemistry* **81**, 5541 (2009).

[18] S. S. Verbridge, J. B. Edel, S. M. Stavis, J. M. Moran-Mirabal, S. D. Allen, G. Coates, and H. G. Craighead, Suspended glass nanochannels coupled with microstructures for single molecule detection, *Journal of Applied Physics* **97**, 124317 (2005).